

Modeling, Simulation, and Control of a Hydraulic Stewart Platform

D. Li and S. E. Salcudean

Department of Electrical Engineering

University of British Columbia

Vancouver, BC, V6T 1Z4, Canada

damingl@ee.ubc.ca, tims@ee.ubc.ca

Abstract

This paper describes the modeling, simulation, and control of an inverted, ceiling-mounted Stewart platform, designed to be a one-person motion simulator. The dynamic equations of the Stewart platform are derived using the virtual work principle. It is shown by simulations that the leg dynamics can be neglected. A model of the electrohydraulic actuator is derived and then verified using experimental data. A link-space pressure-feedback controller is proposed for high performance with good stability robustness. With the above controller, the small-motion position bandwidth of the platform can reach 9Hz along the vertical axis for a payload of about 140 kg.

1 Introduction

To simulate the motion of heavy hydraulic equipment for the purpose of human factors and teleoperation work, a motion simulator was designed and built in the Robotics and Control Laboratory at the University of British Columbia [1, 2]. The simulator shown schematically in Figure 1 is a Stewart platform actuated by hydraulic jacks hanging from the ceiling, and is capable of moving a subject with appropriate displays and hand-controls along six degrees of freedom. The hydraulic actuation system includes a hydraulic power supply unit, a fluid distribution system, and six electrohydraulic actuators. The electrical system includes an electrical signal distribution box, a VME-based real-time system running VxWorks, and a workstation served as user interface. This paper addresses issues of modeling, simulation, and control of such a platform.

Although hydraulic Stewart platforms have been used for years in aircraft simulators, and some are now available commercially, there is not much published work on their dynamics and control. Inverse kinematics has been derived by many researchers based on different coordinate systems. Iterative solutions to the forward kinematics problem have been proposed [8] and evaluated [2, 3]. Do and Yang used Newton-Euler equations of motion to solve the inverse dynamics [5]. Kai Liu *et al* used a Lagrangian approach to derive the dynamic equations in Cartesian-space and then used Jacobian transformations to obtain the ac-

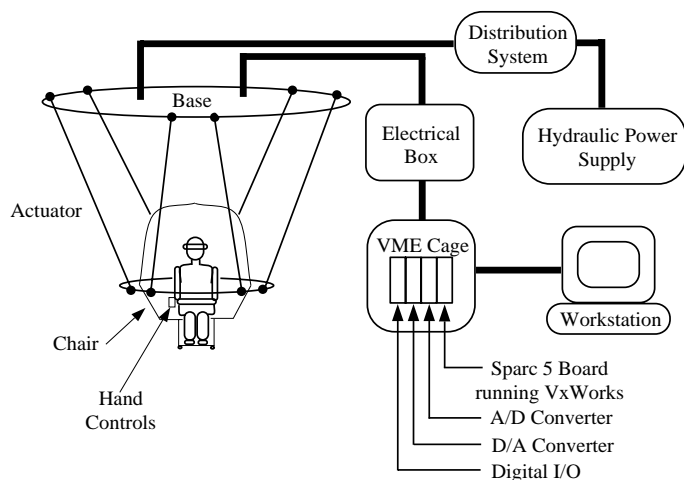


Figure 1: Diagram of the motion simulator system

tuating forces in link-space [7]. Zhang and Song used the virtual work principle to obtain the Stewart platform dynamics, including leg dynamics [4], however, their choice of coordinates is less intuitive, and the dynamics equations are difficult to use in calculating the actuator forces when a Cartesian-space trajectory is given. The control of the Stewart platform based vehicle emulation system at MIT was discussed in [9].

This paper makes the following contributions: (i) the platform dynamics are derived using the principle of virtual work in a simpler way than previously reported ([5], [7], and [4]), and dynamic simulations are then used to show empirically that the platform leg dynamics can be neglected in predicting system trajectories; (ii) a model of the electrohydraulic actuators is obtained and validated experimentally; (iii) a high-performance model-based controller that relies on pressure feedback to ensure the stability of the system is developed and tested experimentally.

The paper is organized as follows. Section 2 reviews the kinematics of the Stewart platform. In Section 3, the platform dynamics are derived and simulation re-

sults are presented with and without considering leg dynamics. Section 4 presents the model of the electrohydraulic actuator, while the control approach, its implementation and experimental results are discussed in Section 5. Section 6 presents conclusions and plans for future work.

2 Kinematics

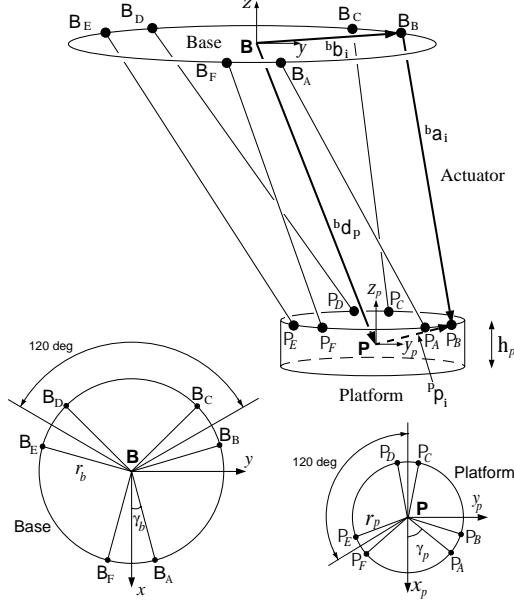


Figure 2: Inverted Stewart Platform

The platform is schematically represented in the above figure, [2], with coordinate frames $\{\mathbf{P}\}$ and $\{\mathbf{B}\}$ attached to the platform and the base, respectively. Each electrohydraulic actuator i has a vector displacement ${}^b\mathbf{a}_i$, pointing from the base attachment point to the platform attachment point, and given in base frame by

$${}^b\mathbf{a}_i = {}^b\mathbf{R}_p {}^p\mathbf{p}_i + {}^b\mathbf{d}_p - {}^b\mathbf{b}_i \quad (1)$$

where ${}^b\mathbf{R}_p$ is the platform rotation matrix and ${}^b\mathbf{d}_p = [x_p, y_p, z_p]^T$ is the platform translation vector, both with respect to the base, and ${}^p\mathbf{p}_i$ and ${}^b\mathbf{b}_i$ are fixed leg offset vectors as shown in Figure 2. The length of the i^{th} actuator is given by $l_i = \|{}^b\mathbf{a}_i\|$ and computing $\mathbf{l} = [l_A, l_B, l_C, l_D, l_E, l_F]$ solves the inverse kinematics of the platform. The following Jacobian transformation gives the velocity kinematics of the platform:

$$\dot{\mathbf{l}} = \mathbf{J} \begin{bmatrix} {}^b\mathbf{v}_p \\ {}^b\boldsymbol{\omega}_p \end{bmatrix} \quad (2)$$

where ${}^b\mathbf{v}_p = \dot{{}^b\mathbf{d}_p}$ and ${}^b\boldsymbol{\omega}_p$ are the translational and rotational velocities of the platform, and each row \mathbf{J}_i , $i = A, B, \dots, F$, of the Jacobian has the form

$$\mathbf{J}_i = \frac{1}{l_i} \begin{bmatrix} {}^b\mathbf{R}_p {}^p\mathbf{p}_i + {}^b\mathbf{d}_p - {}^b\mathbf{b}_i \\ ({}^b\mathbf{R}_p {}^p\mathbf{p}_i) \times ({}^b\mathbf{d}_p - {}^b\mathbf{b}_i) \end{bmatrix}^T \quad (3)$$

Although there is no known closed-form solution to the forward kinematics, the use of Newton's method has been proposed in [8] and elsewhere and shown to work well in practice with a couple of iterations per control sample [3].

The diagram of a platform jack is shown in Figure 3, and consists of two parts: the upper cylinder attached to the base (ceiling), and the lower rod attached to the platform. The lengths l_u and l_l define the centers of mass of the cylinder and the rod. The angular velocity of each leg around its base attachment point is given by

$$\begin{aligned} {}^b\boldsymbol{\omega}_i &= \frac{1}{{}^b\mathbf{a}_i^T {}^b\mathbf{a}_i} {}^b\mathbf{a}_i \times \dot{{}^b\mathbf{a}_i} \\ &= \frac{1}{{}^b\mathbf{a}_i^T {}^b\mathbf{a}_i} {}^b\mathbf{a}_i \times [I, -\mathbf{S}({}^b\mathbf{R}_p {}^p\mathbf{p}_i)] \begin{bmatrix} {}^b\mathbf{v}_p \\ {}^b\boldsymbol{\omega}_p \end{bmatrix} \\ &= \mathbf{t}_i \begin{bmatrix} {}^b\mathbf{v}_p \\ {}^b\boldsymbol{\omega}_p \end{bmatrix} \end{aligned} \quad (4)$$

where $\mathbf{S}({}^b\mathbf{R}_p {}^p\mathbf{p}_i)$ is the skew symmetric matrix of $({}^b\mathbf{R}_p {}^p\mathbf{p}_i)$.

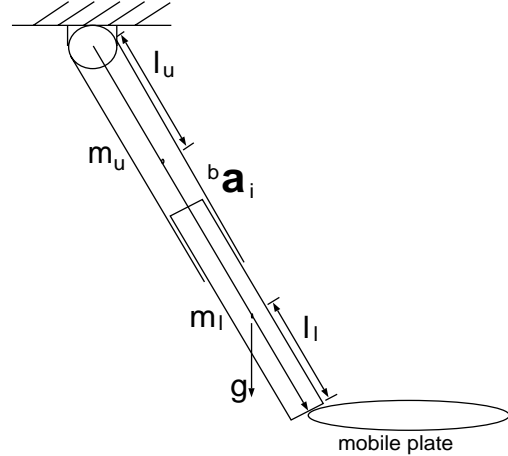


Figure 3: Diagram of leg i

Referring to Figure 3, the cylinder translational velocity ${}^b\mathbf{v}_{il}$ and the rod translational velocity ${}^b\mathbf{v}_{iu}$ are related to the platform velocity by the following Jacobian transformations:

$$\begin{aligned} {}^b\mathbf{v}_{il} &= \frac{l_l {}^b\mathbf{a}_i^T \dot{{}^b\mathbf{a}_i}}{\|{}^b\mathbf{a}_i\| \|{}^b\mathbf{a}_i^T {}^b\mathbf{a}_i\|} {}^b\mathbf{a}_i + \frac{\|{}^b\mathbf{a}_i\| - l_l} {\|{}^b\mathbf{a}_i\|} \dot{{}^b\mathbf{a}_i} \\ &= \left(\frac{l_l} {\|{}^b\mathbf{a}_i\| \|{}^b\mathbf{a}_i^T {}^b\mathbf{a}_i\|} {}^b\mathbf{a}_i {}^b\mathbf{a}_i^T [I, -\mathbf{S}({}^b\mathbf{R}_p {}^p\mathbf{p}_i)] + \frac{\|{}^b\mathbf{a}_i\| - l_l} {\|{}^b\mathbf{a}_i\|} [I, -\mathbf{S}({}^b\mathbf{R}_p {}^p\mathbf{p}_i)] \right) \begin{bmatrix} {}^b\mathbf{v}_p \\ {}^b\boldsymbol{\omega}_p \end{bmatrix} \\ &= \mathbf{h}_{il} \begin{bmatrix} {}^b\mathbf{v}_p \\ {}^b\boldsymbol{\omega}_p \end{bmatrix} \end{aligned} \quad (5)$$

and

$$\begin{aligned}
{}^b \mathbf{v}_{iu} &= \frac{-l_u {}^b \mathbf{a}_i^T {}^b \dot{\mathbf{a}}_i} {\|{}^b \mathbf{a}_i\| \|{}^b \mathbf{a}_i^T {}^b \mathbf{a}_i\|} {}^b \mathbf{a}_i + \frac{l_u} {\|{}^b \mathbf{a}_i\|} \dot{{}^b \mathbf{a}}_i \\
&= \left(\frac{-l_u} {\|{}^b \mathbf{a}_i\| \|{}^b \mathbf{a}_i^T {}^b \mathbf{a}_i\|} {}^b \mathbf{a}_i {}^b \mathbf{a}_i^T [I, -\mathbf{S} ({}^b \mathbf{R}_p^p \mathbf{p}_i)] + \right. \\
&\quad \left. \frac{l_u} {\|{}^b \mathbf{a}_i\|} [I, -\mathbf{S} ({}^b \mathbf{R}_p^p \mathbf{p}_i)] \right) \begin{bmatrix} {}^b \mathbf{v}_p \\ {}^b \omega_p \end{bmatrix} \\
&= \mathbf{h}_{iu} \begin{bmatrix} {}^b \mathbf{v}_p \\ {}^b \omega_p \end{bmatrix} \quad (6)
\end{aligned}$$

The mass of the actuator's upper cylinder, the mass of the actuator's lower rod, and the mass of the mobile platform are defined as m_u , m_l , and m_p , respectively.

3 Platform Rigid Body Dynamics

The virtual work principle will now be used to formulate the rigid body dynamics of the Stewart platform. In the following analysis, actuator and U-joint friction are neglected, since U-joint friction is small, and actuator friction can be incorporated in the hydraulics model, as done in Section 4. It is also assumed that the moment of inertia of leg i about the axis ${}^b \mathbf{a}_i$ is negligible, so that each leg can be modeled as a slender rod.

The virtual work δw , done in translating the platform by a virtual distance ${}^b \mathbf{v}_p \delta t$, rotating the platform by the virtual angle ${}^b \omega_p \delta t$, and rotating the legs by the virtual angles ${}^b \omega_i \delta t$, is

$$\begin{aligned}
\delta w &= m_p {}^b \mathbf{g}^T {}^b \mathbf{v}_p \delta t + \sum_{i=1}^6 (m_l {}^b \mathbf{g}^T {}^b \mathbf{v}_{il} + m_u {}^b \mathbf{g}^T {}^b \mathbf{v}_{iu}) \delta t + \\
&\quad \mathbf{f}^T \mathbf{1} \delta t - \begin{bmatrix} {}^b \mathbf{f}_p \\ {}^b \tau_p \end{bmatrix}^T \begin{bmatrix} {}^b \mathbf{v}_p \\ {}^b \omega_p \end{bmatrix} \delta t - \sum_{i=1}^6 {}^b \tau_i^T {}^b \omega_i \delta t \quad (7)
\end{aligned}$$

where m_p is the platform mass, m_u is the actuator cylinder mass, m_l is the actuator rod mass, \mathbf{g} is the gravity acceleration vector, \mathbf{f} is the six vector of the actuator forces, ${}^b \mathbf{f}_p$ is the force acting on the center of mass of the platform, ${}^b \tau_p$ is the total torque acting about the center of mass of the platform, and ${}^b \tau_i$ is the torque acting about the base attachment point of each leg.

We have

$${}^b \tau_i = (I_{li} + I_{ui}) {}^b \alpha_i \quad (8)$$

where I_{li} is the inertia variable of the lower rod of leg i , I_{ui} is the inertia constant of the upper cylinder of leg i , and ${}^b \alpha_i$ is obtained by taking derivatives of (4),

$${}^b \alpha_i = \mathbf{t}_i \begin{bmatrix} {}^b \mathbf{a}_p \\ {}^b \alpha_p \end{bmatrix} + \dot{\mathbf{t}}_i \begin{bmatrix} {}^b \mathbf{v}_p \\ {}^b \omega_p \end{bmatrix} \quad (9)$$

When the effect of gravity is considered separately, the platform force ${}^b \mathbf{f}_p$ and center-of-mass acceleration ${}^b \mathbf{a}_p$ are related by Newton's law

$${}^b \mathbf{f}_p = m_p {}^b \mathbf{a}_p \quad (10)$$

while the torque on the platform about the center of mass and its angular acceleration ${}^b \alpha_p$ are related by Euler's law

$${}^b \tau_p = {}^b \mathbf{I}_p {}^b \alpha_p + {}^b \omega_p \times ({}^b \mathbf{I}_p {}^b \omega_p) \quad (11)$$

where ${}^b \mathbf{I}_p$ is the platform inertia matrix in base frame.

The principle of virtual work states that the work done by external forces ($\mathbf{f}; {}^b \mathbf{f}_p, {}^b \tau_p$) corresponding to any virtual displacements ($\delta \mathbf{l}; \delta \mathbf{d}, \delta \psi, \delta \theta, \delta \phi$) is zero ($\delta w = 0$) [14]. Substituting (2), (5), (6), and (4) into (7) and applying the principle of virtual work, we then have

$$\begin{aligned}
&\left(\begin{bmatrix} \mathbf{I} \\ 0 \end{bmatrix} m_p {}^b \mathbf{g} + \sum_{i=1}^6 ({}^b \mathbf{h}_{il}^T m_l {}^b \mathbf{g} + {}^b \mathbf{h}_{iu}^T m_u {}^b \mathbf{g}) + \right. \\
&\quad \left. \mathbf{J}^T \mathbf{f} - \begin{bmatrix} {}^b \mathbf{f}_p \\ {}^b \tau_p \end{bmatrix} - \sum_{i=1}^6 ({}^b \mathbf{t}_i^T {}^b \tau_i) \right) \begin{bmatrix} {}^b \mathbf{v}_p \\ {}^b \omega_p \end{bmatrix} \delta t = 0 \quad (12)
\end{aligned}$$

The arbitrary time interval δt and the arbitrary vector $\begin{bmatrix} {}^b \mathbf{v}_p \\ {}^b \omega_p \end{bmatrix}$ can be eliminated. If \mathbf{J} is non-singular, the actuator forces are given by

$$\begin{aligned}
\mathbf{f} &= (\mathbf{J}^T)^{-1} \left(\begin{bmatrix} {}^b \mathbf{f}_p \\ {}^b \tau_p \end{bmatrix} + \sum_{i=1}^6 ({}^b \mathbf{t}_i^T {}^b \tau_i - \right. \\
&\quad \left. \begin{bmatrix} \mathbf{I} \\ 0 \end{bmatrix} m_p {}^b \mathbf{g} - \sum_{i=1}^6 ({}^b \mathbf{h}_{il}^T m_l {}^b \mathbf{g} + {}^b \mathbf{h}_{iu}^T m_u {}^b \mathbf{g}) \right) \quad (13)
\end{aligned}$$

where the expressions of \mathbf{h}_{il} , \mathbf{h}_{iu} , \mathbf{t}_i , ${}^b \tau_i$, ${}^b \mathbf{f}_p$, and ${}^b \tau_p$, can be found in (5), (6), (4), (8), (10), and (11), respectively. This is the complete model of the inverse dynamics of the Stewart platform, which gives the actuator forces in the link-space in terms of the position, velocity, and acceleration of the platform in the Cartesian-space.

For the Stewart platform considered here, the mass of the six legs is considerably smaller than that of the mobile platform. In the rigid body dynamic equations, the leg dynamics part is more complicated and less important than the platform dynamics part. If the leg dynamics are neglected, equation (13) becomes

$$\begin{aligned}
\mathbf{f} &= (\mathbf{J}^T)^{-1} \left(\begin{bmatrix} {}^b \mathbf{f}_p \\ {}^b \tau_p \end{bmatrix} - \begin{bmatrix} \mathbf{I} \\ 0 \end{bmatrix} m_p {}^b \mathbf{g} \right) \\
&= (\mathbf{J}^T)^{-1} \begin{bmatrix} m_p {}^b \mathbf{a}_p - m_p {}^b \mathbf{g} \\ {}^b \mathbf{I}_p {}^b \alpha_p + {}^b \omega_p \times ({}^b \mathbf{I}_p {}^b \omega_p) \end{bmatrix} \quad (14)
\end{aligned}$$

The effect of leg dynamics on actuator forces can be evaluated empirically by simulations. The mobile platform weights about 140 kg, while each leg weights about 15 kg. Several sets of simulations were performed with and without considering the leg dynamics and the required actuator forces were plotted. A typical result, with a trajectory $\ddot{y} = g$ from home position and a sinusoidal pitch angle, is shown in Figure 4. It can be seen that the leg dynamics part counts for less than 10% of total leg forces and can therefore be neglected for most simulations. This simplifies simulation work and real-time control.

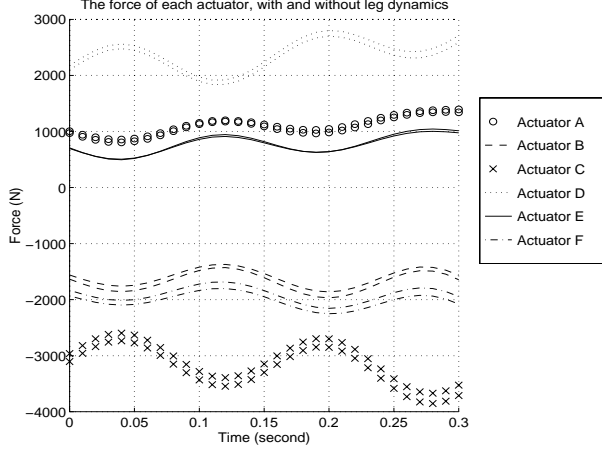


Figure 4: The force of each actuator, with and without considering leg dynamics

4 Actuator Dynamics

Each electrohydraulic actuator consists of an asymmetrical cylinder controlled by a hydraulic valve in a three-way configuration, as shown in Figure 5. Its model depends on the fluid flow through a variable valve opening, the compressibility of the fluid, the load and viscous friction forces, and the dynamic response of the valve [10, 11]. Assuming no leakage, the flow

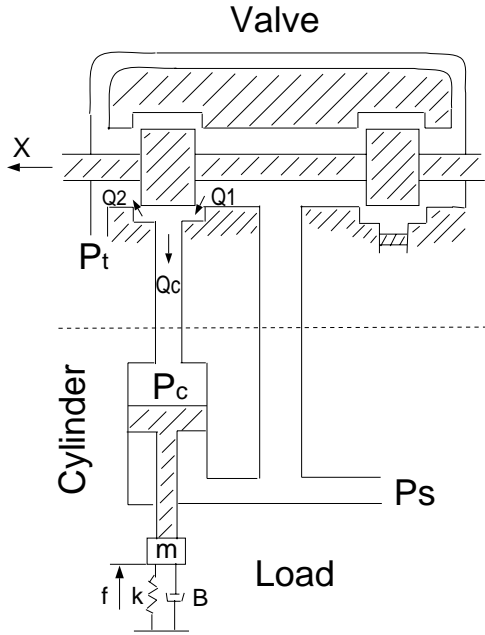


Figure 5: Definition of actuator parameters.

rate Q_c from the valve into the blind end of the cylinder is

$$Q_c = Q_1 - Q_2 \quad (15)$$

where Q_1 is the flow rate from the pressure power supply to the cylinder and Q_2 is the flow rate from the

cylinder to the tank. Assuming turbulent flow[11], Q_1 and Q_2 are given by

$$Q_1 = \begin{cases} C_d w (U + X_v) \sqrt{\frac{2}{\rho} (P_s - P_c)}, & X_v > -U \\ 0, & X_v < -U \end{cases} \quad (16)$$

$$Q_2 = \begin{cases} C_d w (U - X_v) \sqrt{\frac{2}{\rho} (P_c - P_t)}, & X_v < U \\ 0, & X_v > U \end{cases} \quad (17)$$

where C_d is the discharge coefficient, w is the port width of the valve, U is the valve underlap, X_v is the spool position of the valve relative to its center, ρ is the density of the fluid, P_s is the supply pressure, P_c is the controlled pressure at the blind end of the cylinder and $P_t \approx 0$ is the tank pressure.

The compressibility of the fluid can be expressed as

$$V = V_u - \frac{V_u}{\beta} P_c \quad (18)$$

where β is the bulk modulus of the fluid, V is the total volume contained between the piston and the blind end of the cylinder, and V_u is its equivalent uncompressible volume. The transient flow rate associated with fluid compressibility is proportional to the rate of change of pressure and may be expressed as

$$Q_p = \frac{V_u}{\beta} \frac{dP_c}{dt} \quad (19)$$

The flow through the valve is the sum of the flow associated with piston movement and the flow associated with fluid compressibility, or

$$Q_c = \dot{V} + Q_p = \dot{V} + \frac{V_u}{\beta} \dot{P}_c. \quad (20)$$

We can use Newton's law for each cylinder to obtain

$$P_c A - P_s a = M \ddot{l} + B \dot{l} + K l + f \quad (21)$$

where a is the annulus area between the piston rod and the cylinder wall, M is the mass of the load, B is a viscous damping coefficient (normally piston seal friction), K is the spring constant of the load ($K = 0$ for a motion simulator application), and f is an external force.

By differentiating equation (21) and substituting (15), (16), (17) and (20) into the result, we obtain a third order nonlinear equation describing the cylinder extension as a function of spool position, actuator lengths, actuator forces, and system parameters p_{sys} :

$$\ddot{l} = f_{cyl} (l, \dot{l}, \ddot{l}, f, \dot{f}, X_v, p_{sys}) , \quad (22)$$

or

$$\ddot{l} = \frac{1}{M} \left[\frac{\beta A}{V_u} \left(C_d w \sqrt{\frac{2}{\rho} h} (X_v, P_c) - \dot{V} \right) - B \dot{l} - f \right] \quad (23)$$

where, with L the stroke length of the cylinder,

$$V_u \approx A(l - L) / \left(1 - \frac{P_c}{\beta}\right) \quad (24)$$

$$\dot{V} = A\dot{l} \quad (25)$$

$$P_c = \frac{M\ddot{l} + B\dot{l} + Kl + f + P_s a}{A} \quad (26)$$

$$h(X_v, P_c) = \begin{cases} h_1, & X_v > U \\ h_1 - h_2, & -U < X_v < U \\ -h_2, & X_v < -U \end{cases} \quad (27)$$

$$h_1 = (U + X_v) \sqrt{P_s - P_c} \quad (28)$$

$$h_2 = (U - X_v) \sqrt{P_c - P_t} \quad (29)$$

The valve dynamics can be approximately modeled as a second order closed-loop system with the transfer function

$$X_v(s) = \frac{1}{\frac{1}{\omega_e^2} s^2 + \frac{2\xi_e}{\omega_e} s + 1} V_{DA}(s) \quad (30)$$

where V_{DA} is the output of the D/A board, ω_e is the electrical undamped natural frequency and ξ_e is the electrical damping ratio. Note that the above equation, (23), with $M = m_l$, and (14) and its derivative can be combined to obtain the full nonlinear dynamics of the Stewart platform, including rigid body and hydraulic dynamics, in link-space. Cartesian-space formulations would be implicit since the inverse kinematics has no closed-form solution. A linearized multivariable model can be obtained and multivariable controllers can be designed using standard approaches, but the resulting systems would be of substantial complexity and of little intuitive value. Therefore, the control study presented here addresses only the single cylinder control. Studies to determine the robustness of such decoupled controllers to platform rigid-body and flexible dynamics will be conducted in the future.

The linear model of a single cylinder is given by the following fifth order system:

$$L(s) = \frac{\frac{K_q}{A} V_{DA}(s)}{s \left(\frac{1}{\omega_h^2} s^2 + \frac{2\xi_h}{\omega_h} s + 1 \right) \left(\frac{1}{\omega_e^2} s^2 + \frac{2\xi_e}{\omega_e} s + 1 \right)} - \frac{\frac{V_0}{A^2 \beta} F(s)}{\frac{1}{\omega_h^2} s^2 + \frac{2\xi_h}{\omega_h} s + 1} \quad (31)$$

where $\omega_h = A\sqrt{\frac{\beta}{V_0 M}}$ is the hydraulic undamped natural frequency and $\xi_h = \frac{B}{2A}\sqrt{\frac{V_0}{\beta M}}$ is the hydraulic damping ratio.

By using low-pass filtered white noise as the valve input signal [15], we obtained the D/A command value to valve opening transfer function shown in Figure 6 and the valve opening to actuator length transfer function shown in Figure 7 with good coherence measures. Results show that the linearized actuator model

and the experimental data fit each other well. Details about the system parameters can be found in [3].

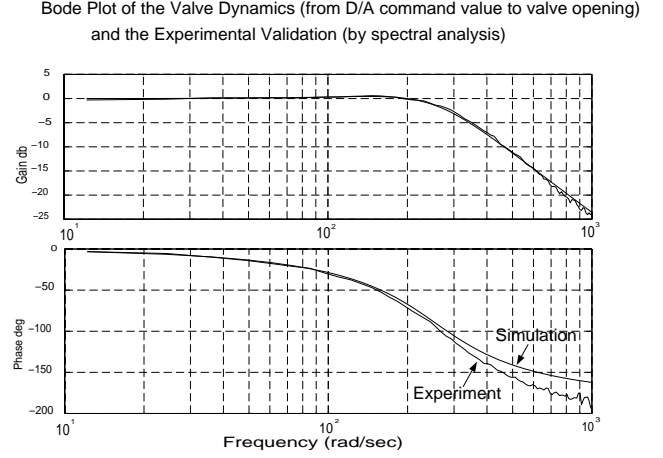


Figure 6: Linearized valve model and the validation

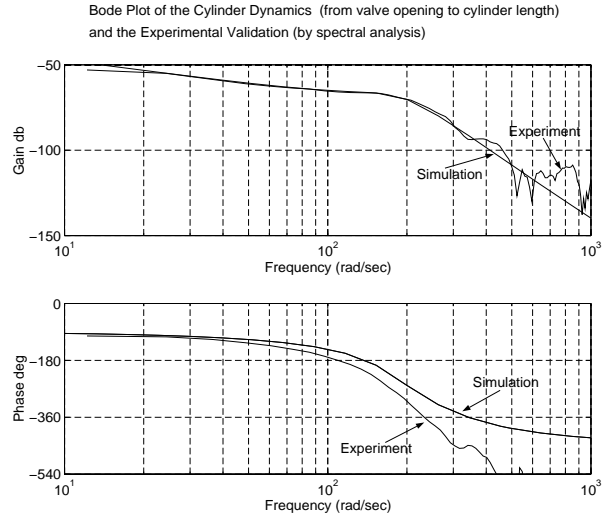


Figure 7: Linearized cylinder model and the validation

5 Controller Design and Results

A proportional gain controller is the simplest way to control the position of the electrohydraulic actuator, as its transfer function is nearly an integrator at low frequencies. Such a controller was implemented and lead to rather poor performance, primarily because the gain could not be increased enough without the bulk modulus resonance causing the closed-loop system to go unstable. It will be shown in the following that negative pressure feedback is an effective way of allowing much higher proportional gains. The argument is based on an analogy to motor shaft control. It is well known that the end-point position control of a mass actuated by a motor through a flexible transmission has much poorer stability robustness than motor-shaft position control [14]. When the motor-shaft po-

sition is not directly available, it can be computed by measuring the end-point position and the stress on the motor shaft. A similar approach can be applied to the control of electrohydraulic actuators, where the compressibility of fluid is analogous to the flexibility of transmission, the actuator length is analogous to the end-point position, and cylinder pressure measurement is analogous to the stress measurement on the motor shaft.

The actuator model presented in Section 4 is now revised to explain this new type of controller design that uses V_u , the equivalent uncompressed volume of fluid trapped between the valve opening and the blind end of the cylinder, as an intermediate variable.

From the compressibility equation (18) and the flow equation (20), Q_c and V_u are related by

$$Q_c = \dot{V}_u \left(1 - \frac{P_c}{\beta}\right) \quad (32)$$

Substituting Newton's law (21) (with $K = 0$) in (18) and using

$$V = A(l - L) \quad (33)$$

we can get

$$A(l - L) = V_u \left(1 - \frac{1}{\beta A} (P_s a + M\ddot{l} + B\dot{l} + f)\right) \quad (34)$$

or

$$\frac{A}{1 - P_s a / A\beta} \left(\frac{V_u M}{A^2 \beta} \ddot{l} + \frac{V_u B}{A^2 \beta} \dot{l} - (l - L) \right) + \frac{V_u}{A\beta - P_s a} f = V_u \quad (35)$$

When V_u is constant, i.e. $Q_c = 0$, the actuator behaves like a spring-damper system. Otherwise, we can consider the actuator model as a spring damper model with slowly-varying parameters. The uncompressed fluid volume V_u and the external force f are the inputs, while the length $(l - L)$ is the output. The linearized actuator model is given by

$$L(s) = \frac{K_v V_u(s) - K_f F(s)}{\omega_n^2 s^2 + \frac{2\xi}{\omega_n} s + 1} \quad (36)$$

where $\omega_n = A\sqrt{\frac{\beta}{V_u M}}$ is the undamped natural frequency, $\xi = \frac{B}{2A}\sqrt{\frac{V_u}{\beta M}}$ is the damping ratio, $K_v = \frac{1 - P_s a / A\beta}{A}$ is the volume gain, and $K_f = \frac{V_u}{A^2 \beta}$ is the force gain.

If the measurement of uncompressed fluid trapped in the cylinder, V_u , rather than the end-point position of the cylinder, l , is to be used as the feedback signal, the desired uncompressed volume is set to

$$V_{ud} = A(l_d - L) \quad (37)$$

where l_d is the desired actuator length. The proportional control law is given by

$$X_v = K_p (V_{ud} - V_u) \quad (38)$$

Substituting (18), (33) and (37) into the above equation and assuming $\beta \gg P_c$, we have

$$X_v = K_p A(l_d - l) - \frac{K_p A(l_d - L)}{\beta} P_c \quad (39)$$

a proportional gain controller with negative pressure feedback.

In the presence of the negative pressure feedback, the proportional gain position controller can be operated with gains that are as much as four or five times higher than without pressure feedback. A set of experimental results showing platform motion along a horizontal axis is shown in Figures 8 and Figure 9. The commanded position is a 1.0 Hz sinusoid of 0.05 meter amplitude. Position tracking of small signals up to 9 Hz have been observed with a nominal platform payload of 140 kg. Software simulations have given similar results.

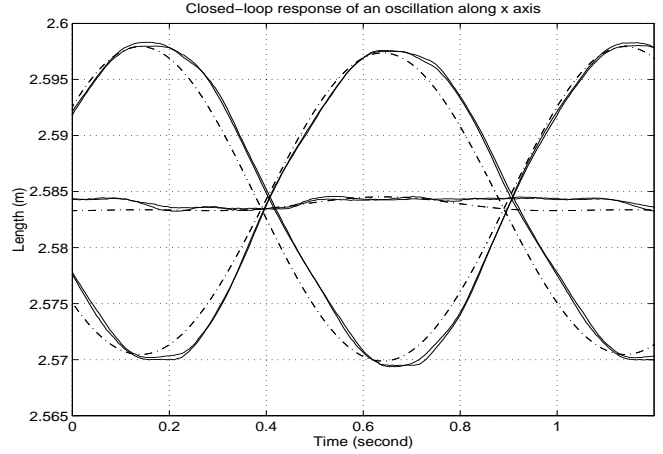


Figure 8: Actuator lengths, sine wave along x axis

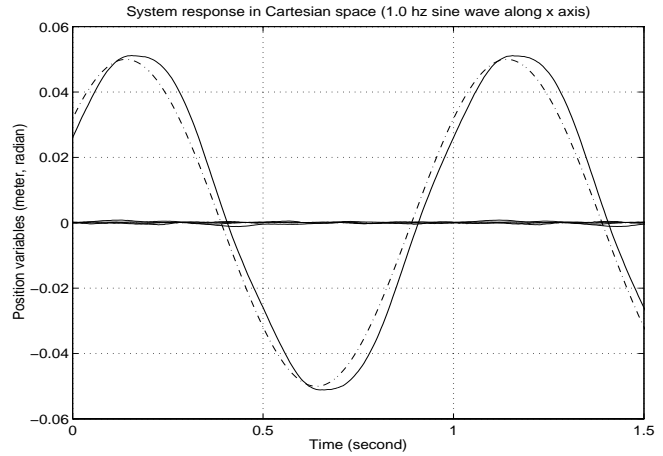


Figure 9: Cartesian-space tracking, sine wave along x axis

6 Conclusion and Future Work

Modeling and control issues of a hydraulically actuated Stewart platform have been discussed. The platform rigid-body and hydraulic dynamics have been presented. It was shown through simulations that the leg dynamics can be neglected in this particular platform design. A negative pressure feedback controller was presented that allows very high proportional position error gains without compromising stability. Experimental results indicate that the frequency response of the Stewart platform using pressure-feedback control is very good. This intuitive and simple approach could be useful in a wide range of hydraulics applications.

The use of on-line identification to determine the bulk modulus value and therefore the pressure gain will be investigated in the future. So will the robustness of the proposed scheme to measurement errors. The effects of leg flexibility and platform rigid-body dynamics on the link-space controllers will be examined analytically and experimentally. The possibility of applying Cartesian space controllers is also of interest.

7 Acknowledgements

The Authors would like to thank Alison Taylor, Simon Bachmann, and Icarus Chau for their contributions to the project. This work was supported by the Canadian IRIS/PREARN Network of Centers of Excellence.

References

- [1] P.A. Drexel, "A Six Degree-of-Freedom, Hydraulic, One Person Motion Simulator," Master's thesis, The University of British Columbia, 1992.
- [2] S.E. Salcudean et al, "A Six Degree-of-Freedom, Hydraulic, One Person Motion Simulator," *Proceedings of the 1994 IEEE International Conference on Robotics and Automation*, 2437-2443, 1994.
- [3] D. Li, "Modeling, Simulation, and Control of a Stewart Platform," Master's thesis, The University of British Columbia, 1997.
- [4] C.D. Zhang and S.M. Song, "An Efficient Method for Inverse Dynamics of Manipulators Based on the Virtual Work Principle," *Journal of Robotic Systems*, 10(5), 605-627, 1993.
- [5] W.Q.D. Do and D.C.H. Yang, "Inverse Dynamic Analysis and Simulation of a Platform Type of Robot", *Journal of Robotic Systems*, 5(3), 209-227, 1988.
- [6] D. Stewart, "A Platform with Six Degrees of Freedom," *Proceedings of the Institution of Mechanical Engineers*, 180(15), 371-386, 1965-1966.
- [7] K. Liu, Mick Fitzgerald, Darren M. Dawson, Frank L. Lewis, "Modeling and Control of a Stewart Platform Manipulator," *American Society of Mechanical Engineers, Dynamic Systems and Control Division (Publication) DSC v 33*, 83-89, 1991.
- [8] J.E. Dieudonne et al, "An Actuator Extension Transformation for a Motion Simulator and an Inverse Transformation applying Newton-Raphson's Method," Technical Report D-7067, NASA, 1972.
- [9] William K. Durfee, Husni R. Idris, and Steven Dubowsky, "Real-Time Control of the MIT Vehicle Emulation System," *Proceedings of the 1991 American Control Conference*, 1991.
- [10] T.J. Viersma, *Analysis, Synthesis, and Design of Hydraulic Servo Systems and Pipelines*, Elsevier Publishing Company, Amsterdam, New York, 1980.
- [11] H.E. Merritt, *Hydraulic Control Systems*, Wiley and Sons, New York, 1967.
- [12] Prabjot Nanua and Kenneth J. Waldron, "Direct Kinematic Solution of a Stewart Platform," *IEEE Transactions on Robotics and Automation*, 431-436, 1989.
- [13] V.E. Gough, "Contribution to discussion to papers on research in automobile stability and control in tyre performance, by Cornell staff," *Proc. Auto. Div. Inst. mech. Engineers*, 171, 392-394, 1956-1957.
- [14] Mark W. Spong and M. Vidyasagar, *Robot Dynamics and Control*, John Wiley & Sons, New York, 1989.
- [15] Athanasios Papoulis, *Probability, Random Variables, and Stochastic Processes*, McGraw-Hill Book Company, New York, 1965.
- [16] J.-J. E. Slotine and Weiping Li, *Applied Nonlinear Control*, Prentice-Hall Inc., New Jersey, 1991.